Diamond Pixel Modules and the ATLAS Beam Conditions Monitor

D. Dobos*[,a], Heinz Pernegger[a], on behalf of the RD42, the ATLAS Diamond Pixel Upgrade and the ATLAS Beam Conditions Monitor Collaborations

[a] *CERN, CH-1211 Geneve 23, Switzerland*

Abstract

Chemical vapour deposition diamonds are considered among possible sensor materials for the next pixel upgrade in ATLAS. Full size diamond pixel modules have been constructed to the specification of the ATLAS Pixel Detector using poly-crystalline CVD diamond sensors to develop the production techniques required for industrial production. Those modules were tested in the lab and testbeam. Additionally we will present results of diamond pixel modules using single-crystal diamonds and results of proton irradiations up to 1.8×10^{16} protons/cm^2. The ATLAS Beam Conditions Monitors (BCM) main purpose is to protect the experiments silicon tracker from beam incidents. In total 16 1×1 cm^2 500 μm thick diamond pCVD sensors are used in eight positions around the LHC interaction point. They perform time difference measurements with sub nanosecond resolution to distinguish between particles from a collision and spray particles from a beam incident; an abundance of the latter can lead the BCM to provoke an abort of LHC beam. The BCM diamond detector modules, their readout system and the algorithms used to detect beam incidents are described. Results of the BCM operation with circulating LHC beams and its commissioning with first LHC collisions are reported.

Key words: CVD diamond, Beam conditions monitor, Pixel detector, LHC, ATLAS experiment

1. ATLAS Diamond Pixel Modules

1.1. Motivation

With the first LHC run in 2009 and upgrades of the tracking detectors expected several years later, the LHC experiments are engaged in R&D for future pixel detector sensor technologies with outstanding radiation hardness. Chemical Vapor Deposition (CVD) diamond has been used extensively in beam conditions monitors as the innermost detectors in the highest radiation areas of BaBar, Belle, CDF and now all LHC experiments. Diamonds are considered as an alternate sensor for use very close to the interaction region of the super LHC where the most extreme radiation conditions will exist. Recently the RD42 collaboration [1] constructed, irradiated and tested polycrystalline and single-crystal chemical vapor deposition diamond pixel sensors towards the specification of the ATLAS diamond pixel sensors [2] and ATLAS Insertable B-Layer upgrade [3].

1.2. Diamond Pixel Sensors

The innermost layers of tracking detectors are currently equipped with high-resolution hybrid pixel detectors for tracking at high particle density. In order to develop and test the techniques required in the construction of a state-of-the-art pixel detector based on CVD diamonds, several full ATLAS diamond pixel modules have been constructed and tested [4]. The diamond pixel modules follow the specification of the ATLAS pixel detector [5, 6]. The sensors are 0.8 mm thick poly-crystalline CVD diamonds with a charge collection distance of ≈250 μm. They are patterned with 50×400 μm sized electrodes on the chip side and a continuous bias contact on the other side where the bias voltage, typically in the range of 400 V to 800 V, is applied. The sensor active area measures 61×16.5 mm^2 and is readout by 16 FEI3 [6] pixel front-end chips. Figure 1 shows an exploded view of the ATLAS diamond pixel module. Chip and sensor electrodes are connected through solder bump-bonding. During the module construction it was demonstrated that the diamond sensor could be fully recuperated, in case the diamond module did not pass the acceptance tests: The front-end chips were removed, the metallization on the diamond sensor was removed and reapplied and new chips remounted to the original sensor. For the test with single-crystal CVD diamonds, dedicated pixel assemblies with one FEI3 bonded to the single-crystal CVD diamond sensor have been prepared as well.

1.3. Testbeam results with full size diamond pixel modules

After module construction the full-size pixel module is calibrated and characterized in laboratory measurements. During the calibration the channel discriminator thresholds are equalized across the module and the equivalent noise charge (ENC noise) is measured for each channel. The module calibration for the diamond pixel module yields a threshold of 1450±25 e$^-$ and an ENC noise of 137±10 e$^-$ for a standard pixel. When the same calibration is carried out on a bare front-end chip, i.e. without sensor connected, we obtain a threshold of 1497±26 e$^-$ and an ENC noise of 138±8 e$^-$ for the chip only. The fact that the sensor is "invisible" to the FE chip is due to the low capacitance and leakage current of diamond sensors. The module was subsequently tested at DESY in a 4 GeV electron testbeam. Figure 2 shows the residual distribution of predicted mi-

*Corresponding author. Tel.: +41-(0)76-487-2297.
Email address: daniel.dobos@cern.ch (D. Dobos)

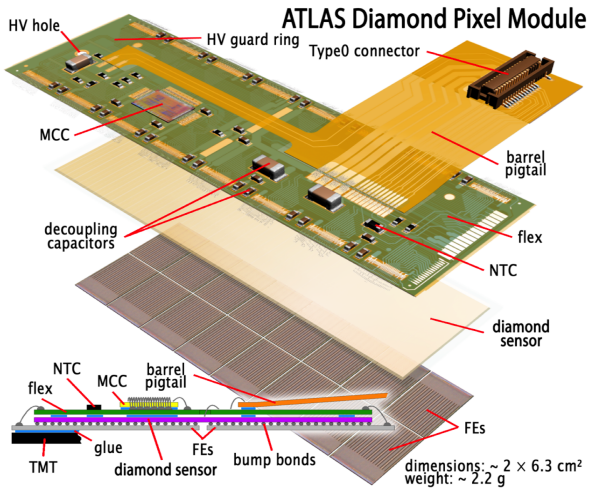

Figure 1: Exploded view of the ATLAS diamond pixel module. The design, construction and components are, with the exception of the sensor, identical to the pixel module which are used currently in the ATLAS Pixel Detector.

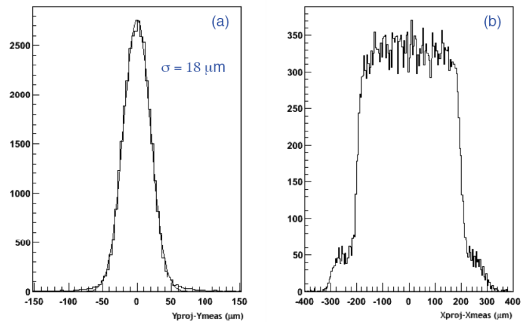

Figure 2: Residual distribution of predicted minus measured hit position along the narrow pad dimension, plot (a), and along the long pad dimension, plot (b)

nus measured hit position along the narrow pad dimension (a) and along the long pad dimension (b). Unfolding the hit prediction uncertainty from the measured residual distribution r.m.s. yields a detector spatial resolution of 14 μm, compatible with the expected resolution of pad width divided by $\sqrt{12}$.

1.4. Test of irradiated diamond pixel sensors

Both poly-crystalline and single-crystal CVD diamonds have been tested in testbeams after irradiation up to fluences of 1.8×10^{16} protons/cm^2. The irradiation has been carried out at the CERN PS with 24 GeV protons. Figure 3 shows the signal distribution, as measured by the FEI3 chip time-over-threshold in a CERN SPS testbeam, for a single crystal CVD diamond pixel detector. The top plot shows the response for the unirradiated detector, which was operated at 400 V bias. The calibration yields a most probable signal of 11540 e$^-$. The bottom plot shows the same detector after irradiation with 0.7×10^{15} protons/cm^2. The irradiated detector was operated at 800 V for an increased signal amplitude. The most probable signal corresponds to a signal charge of 9025 e$^-$.

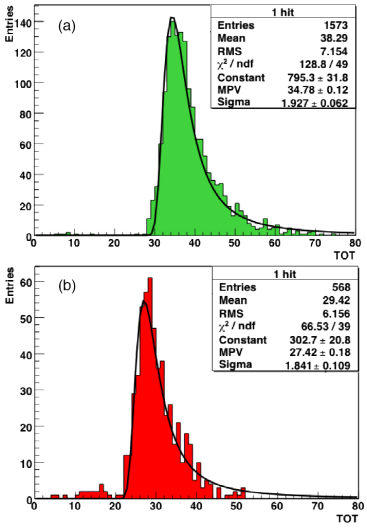

Figure 3: Signal distribution of an unirradiated (a) and irradiated (b) single-crystal diamond pixel detector as measured in the testbeam.

Figure 4 shows the charge collection distance of single-crystal and poly-crystalline CVD diamond strip and pixel detectors after irradiation with 24 GeV protons to fluences of 1.8×10^{16} protons/cm^2. The data points give the charge collection distance as measured in testbeams. To allow the comparison of single-crystal and poly-crystalline CVD diamonds in the same figure, the data points for single-crystal diamonds have been shifted to the left in order to normalize for the different initial charge collection distance of unirradiated samples. This shift of 3.8×10^{15} protons/cm^2 for strip scCVD (3.2×10^{15} protons/cm^2 for pixel scCV) normalizes the charge collection distance to the reference poly-crystalline sample with a charge collection distance of of 215 μm, i.e. the single crystal diamond with an initial charge collection distance of 470 μm will reach a charge collection distance of 215 μm after an irradiation with 3.8×10^{15} protons/cm^2. Single-crystal and poly-crystalline CVD diamonds follow approximately the same damage curve (dotted line) which can be parameterized as

$$ccd = \frac{ccd_0}{1 + 0.7 \cdot 10^{-18} \cdot \Phi \cdot ccd_0} \quad (1)$$

for these data. ccd_0 denotes the initial charge collection distance of 215 μm for the reference poly-crystalline sample and Φ the proton fluence.

2. ATLAS Beam Conditions Monitor

2.1. Motivation

Experiences at previous accelerators and simulations for the ATLAS experiment teach that it is necessary to protect the innermost detector layers from beam incidents. They can lead to detector damage due to high instantaneous radiation doses. A bunch-by-bunch beam conditions measurement with the ATLAS BCM[7] can distinguish between normal collisions, beam

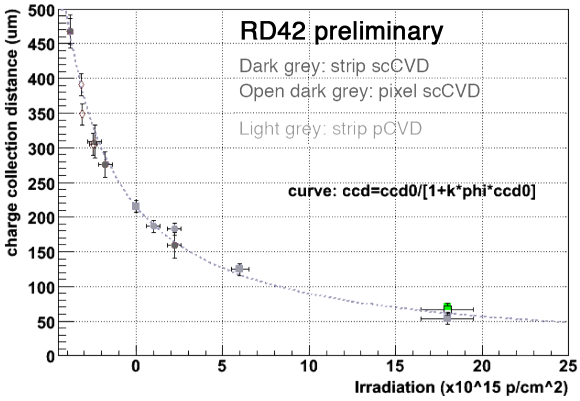

Figure 4: Charge collection distance as function of proton fluence. The charge collection distance has been measured in the testbeam at a detector bias of 1V/μm. The data points of single-crystal diamonds have been shift by 3.8×10^{15} protons/cm^2 for strip scCVD and 3.2×10^{15} protons/cm^2 for pixel scCVD. This shift of horizontal axis between single-crystal and poly-crystalline diamonds normalizes the charge collection distance to the reference poly-crystalline sample with a charge collection distance of of 215 μm.

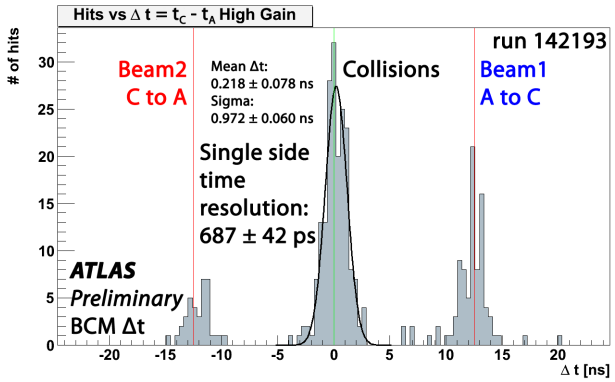

Figure 5: TOF distribution between the two detector stations located at z=±1.84 m. Δt values of 12.5 ns represent beam background events from LHC Beam 1 whereas Δt values of -12.5 ns represent LHC Beam 2 background events, respectively. Collision events have Δt values of 0 ns. A Gaussian fit of the collision peak in the t_C - t_A TOF distribution yields a width of 972 ps; this is consistent with a single side time resolution of 687 ps.

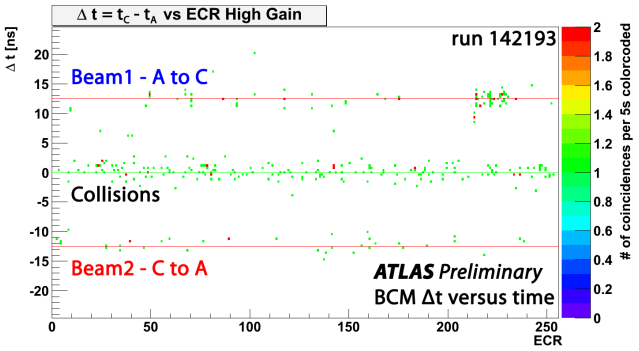

Figure 6: Time evolution of beam background and collision events. The time is binned in units of ECR, which are 5 s signals. The ECR itself is reset approximately every 21 minutes. Since the run was almost 6 hours long, the plot shows a superposition of about 18 ECR sweeps. A higher beam background period for Beam1 is visible between ECR values 210 and 230.

gas, beam halo, pilot beam loss (5×10^9 protons at 450 GeV) and beam loss ($2808\times1.15\times10^{11}$ protons at 7 TeV) events.

The time constant for the effective change of LHC magnet fields is in the order of some ms, which gives enough time to generate beam abort signals preventing the beam incident to happen. The most probable beam incident scenario in ATLAS is a scraping of the pilot bunch at the Target Absorber Secondaries (TAS) collimator 18 m away from the interaction point. This creates a spray of particles depositing a dose of 5×10^{-3} Gy in the Inner Detector volume.

2.2. *BCM Diamond Detectors*

Two detector stations located at positions z=±1.84 m along the beam pipe contain four BCM detectors each. The diamond sensors are mounted with a radius of 5.5 cm above, below, left and right of the beam pipe. Each BCM detector contains two pCVD diamond sensors glued back-to-back to an alumina ceramic board. The sensor material was developed by the CERN RD42 Collaboration[8] and Diamond Detectors Ltd.[9]. Sensors of 1×1 cm^2 and 500 μm thickness have Ti-Pt-Au 8×8 mm^2 contacts on both sides. With 1 kV bias voltage typical sensors have a charge collection distance of 220 μm and a leakage current below 100 pA. The double sensor layout doubles the charge signal with a noise increase of only 30%. With respect to the beam axis the sensors are mounted tilted at 45°. With a most probable MIP energy loss of 9.0 ke$^-$ (mean: 11.3 ke$^-$) signal/noise ratios of ~10 are achieved.

The copper plated module boxes contain two RF current amplifiers with ~20 dB amplification each. The amplifier radiation hardness was qualified with reactor neutrons and protons up to fluences of 10^{15}/cm^2. The signals are routed via 14 m long coaxial cables to readout electronics outside the Hadronic Calorimeter, where the signal is split with a ratio of 1:11 (low and high gain: LG and HG) to increase the dynamic range of the measurement. Both signals are amplified in a NINO[10] chip. Discriminators with adjustable thresholds digitize the signals to encode the charge seen at the input to a Time-Over-Threshold (TOT) length of a LVDS digital pulse, which is sampled with 2.56 GS/s resolution (390 ps sampling period) with a Virtex4 FPGA based Readout Driver (ROD) data acquisition system.

2.3. *LHC 2009 Run Results*

Collision Time-of-Flight (TOF) measurements between the 3.68 m apart stations results in $\Delta t=t_C-t_A$ values of 0 ns, whereas beam background events result in TOF values of ±12.5 ns depending on the direction of particles. The TOF distribution for an example run is shown in Fig.5 showing clear separation between background and collision events. The side to side time resolution determined from the fit of the collisions peak results in 972 ps, which is consistent with a single side time resolution of 687 ps. Fig.6 shows the Δt distribution versus time, which allows to identify periods of high background activity. The Δt distribution versus Bunch Crossing Identifier is shown in Fig.7 exposing the LHC fill structure.

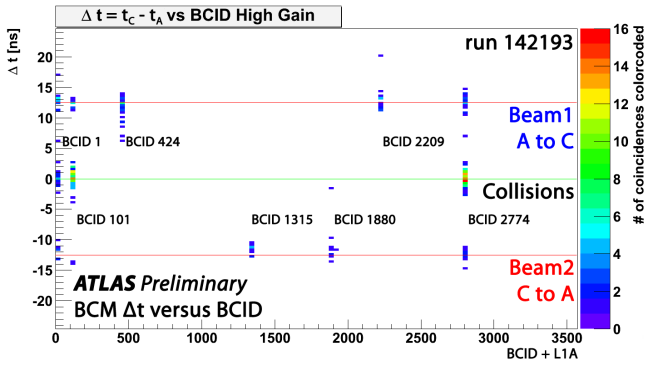

Figure 7: Collision and beam background events as function of the BCID showing the LHC fill structure. Beam background and collision events are visible for bunch crossings with the IDs 1, 101 and 2774. Bunch crossings 424 and 2209 have only beam background events from Beam 1; 1315 and 1880 only from Beam 2. These bunch crossings were setup for collisions in ALICE and LHCb.

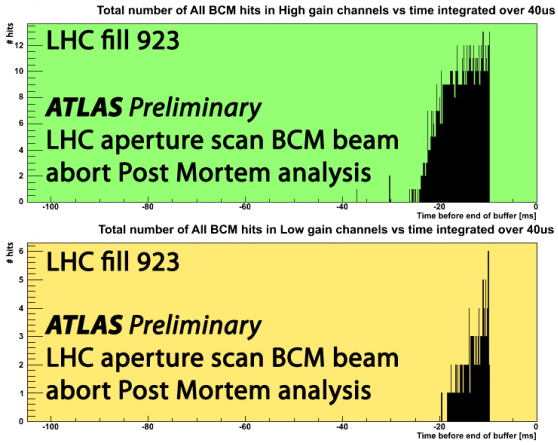

Figure 8: Number of high and low gain channel hits integrated over 40 μs versus time during a LHC Beam 2 IR1 horizontal aperture scan. The post mortem buffer covers 1177 LHC revolutions (105 ms). It is frozen 9 ms (~100 orbits) after an abort. An increase of the number of BCM hits is visible during a step of the aperture scan starting at -26 ms before the end of the buffer. A beam abort initiated by BCM occurred at -9.8 ms before the end of the buffer and the BCM hit activity returns to zero after the beam is dumped.

A circular raw data buffer covers 1177 LHC orbits (105 ms) and is frozen 9 ms (~100 orbits) after a beam abort post mortem signal was received. Fig.8 shows the hits integrated over 40 μs during a LHC Beam2 IR1 horizontal aperture scan step. An increase of high and low gain hits is visible as well as a fast decrease caused by a BCM initiated beam dump. The timelines of the 16 BCM channels in the bunch crossing is shown in Fig.9 reaching the 3 HG + 3 LG beam abort condition for each ROD.

3. Conclusions

Diamond pixel modules have been assembled to specifications of the ATLAS Pixel Detector using the 16 FEI3 front-end chips per module. Calibration results showed excellent noise performance of 137 e^- ENC and an operation threshold of 1450±25 e^-, which we found to be identical to the bare chip test

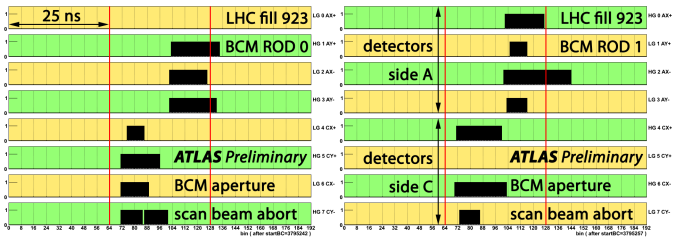

Figure 9: Timelines of the readout channels in full 390 ps sampling resolution covering 3×25 ns bunch crossings. The are recorded with the post mortem buffer during a LHC Beam 2 IR1 horizontal aperture scan in the moment of a BCM initiated beam abort. The left timelines are recorded by one, the right by another ROD. High gain (HG) channel timelines have a green, low gain (LG) ones a yellow background. The top four timelines are from A side detectors, the bottom four from C side detectors. The 3 HG + 3 LG beam abort condition was reached for both RODs and the HG channel show, as expected, longer pulse widths. The pulses of the C side detectors are about 12.5 ns before the A side detector pulses as expected for beam background from Beam 2 (C to A).

results. The module has been tested in an electron test beam at DESY and showed a spatial resolution of 14 μm. Test beam results of irradiated chemical vapor deposition diamond up to fluences of 1.8×10^{16} protons/cm^2 show that both polycrystalline and single-crystal chemical vapor deposition diamonds follow a single damage curve. The BCM showed in the LHC 2009 run excellent TOF side to side time resolution, which is consistent with a single side time resolution of 687 ps. Periods of high beam background activity and the bunch fill structure of the LHC were identified. The 1177 LHC orbit beam abort buffer allows to monitor the course of abort beam losses in ATLAS and provides beam abort diagnostics. The BCM timing is sufficient to use TOF based beam abort algorithms soon.

References

[1] The RD42 Collaboration, R&D Proposal, "Development of Diamond Tracking Detectors for High Luminosity Experiements at LHC", DRDC/P56, CERN/DRDC 94-21, May 1994.

[2] CERN EDMS document 903424, ATU-RD-MN-0012, https://edms.cern.ch/document/903424/1, March 2008.

[3] T. Flick, "IBL ATLAS Pixel Upgrade", ATL-INDET-PROC-2010-001, Proceedings of Science, Vertex 2009, January 2010.

[4] M. Mathes, "Development and characterization of diamond and 3D-silicon pixel detectors with ATLAS-pixel readout electronics", PhD thesis, Universität Bonn, Bonn IR 2008 15, 2008

[5] G. Aad et al., "The ATLAS Collaboration", The ATLAS Experiment at the CERN Large Hadron Collider, JINST 3 (2008) S08003.

[6] G. Aad et al., "ATLAS pixel detector electronics and sensors", JINST 3 (2008) P07007.

[7] ATLAS BCM Collaboration, The ATLAS Beam Conditions Monitor, 2008 JINST 3 P02004.

[8] CERN RD42 collaboration: "CVD Diamond Radiation Detector Development". - RD42 Status Report: Development of Diamond Tracking Detectors for High Luminosity Experiments at the LHC, LHCC-RD-016, CERN-LHCC-2008-005.

[9] Diamond Detectors Ltd., Upton Road, Poole, Dorset, UK.

[10] NINO: an ultra-fast and lowpower frontend amplier and discriminator ASIC for the multi-gap resistive plate chambers, F. Anghinol et al., Nucl. Instr. Methods A, 533:183187, 2004.